Supplementary Information

Coupling Interfacial Electron Polarization with Carbonate-Mediated Proton Relay for Efficient CO_2-to-CO Electrocatalysis

Xin Cui [a,#], Xianyong Li[b,#], Teng Zhang[a], Yilin Yin[b], Gaowu Qin[c], Song Li [a,*]

[a] *School of Materials Science and Engineering, Northeastern University, Shenyang 110819, China*

[b] *Golden Sea Research Institute of Chemical Industry, Tianjin 300280, China*

[c] *Institute for Strategic Materials and Components, Shenyang University of Chemical Technology, Shenyang 110142, China*

[#] These authors contributed equally to this work.

* Email: lis@neu.edu.cn

Experimental

Materials and reagents

Cadmium acetate dihydrate ($(CdCH_3COO)_2 \cdot 2H_2O$, 99 %, AR), silver nitrate ($AgNO_3$, 99%, AR) and ethylene glycol (EG, 99%, AR) were purchased from Sinopharm Chemical Reagent Co., Ltd. Polyvinylpyrrolidone (PVP, average M_w = 58000), ferric chloride ($FeCl_3$, 98%, AR) and acetone (AC, 99.5%, AR) were supplied by Shanghai Aladdin Chemical Co., Ltd. Sodium chloride (NaCl, 99.9%, AR) and ethyl alcohol (C_2H_5OH, 99.7%, AR) were provided by Tianjin Feng-chuan Chemical Reagent Technologies Co., Ltd.

Preparation of Ag nanowires (NWs)

Ag NWs were synthesized using a modified polyol process.[1] In a typical experiment process, 20 mL of EG was poured into a three-necked flask and preheated in a 170 ℃ oil bath with constant stirring for 5 min to remove moisture. Subsequently, 0.34 g of PVP was added to the three-necked flask and stirred at 800 rpm. The resulting mixed solution was maintained at 170 ℃ for 10 min. Next, an excess amount of freshly prepared AgCl (25 mg) was added to the above solution all at once, causing the solution to change from transparent to light yellow. After allowing the reaction to proceed for 3 min, 0.11 g of $AgNO_3$ was added to the mixture in one go. The reaction mixture solution was continuously stirred at 170℃ for 30 min. Finally, the resulting products were collected by centrifugation and washed several times with ethanol and deionized water.

Preparation of silver chloride nanowires (AgCl NWs)

AgCl NWs were prepared via galvanic replacement reaction (GRR) method between Ag NWs and $FeCl_3$ according to a previously reported literature.[2] Briefly, 200 μL of 0.5 M $FeCl_3$ solution was added dropwise into 2 mL of Ag NWs dispersion liquid (10 mg/mL in water). The obtained solution was continuously stirred for 15 min until the solution turned light purple, indicating the formation of AgCl NWs. The target products were collected by centrifugation and washed with deionized water for several times. Finally, the obtained precipitates were dried in a vacuum oven at 50 ℃ for 12 h.

Preparation of $CdCO_3$/AgCl NWs, $CdCO_3$/Ag NWs, $CdCO_3$ + AgCl NWs and $CdCO_3$

The $CdCO_3$/AgCl NWs were synthesized by in-situ growth method. First, 0.05 g AgCl NWs were added into 20 mL deionized water with constant stirring for 15 min to obtain solution A, while 1.0 mmol $Cd(CH_3COO)_2 \cdot 2H_2O$ was dissolved into 10 ml deionized water under stirring to get solution B. Then, the solution B was added dropwise into solution A under vigorous stirring. After continually stirring for about 30 min, CO_2 was pumped into the mixture at a flow rate of 25 mL/min for 20 min. Finally, the resulting precipitate was collected through centrifugation and washed multiple times with deionized water. The precipitates were dried in

a vacuum oven at 50℃ for 12 h.

Similarly, the synthetic process of $CdCO_3$/Ag NWs and $CdCO_3$ is quite similar to that of $CdCO_3$/AgCl NWs, except that solution A is replaced with Ag NWs and without adding A solution, respectively.

To prepare the physically mixed $CdCO_3$ + AgCl NWs catalyst, $CdCO_3$ and AgCl NWs were added to a solution and stirred continuously for 30 min. The mass ratio of the two components was controlled to be identical to that in the $CdCO_3$/AgCl NWs heterojunction.

Preparation of the working electrode

The working electrodes were fabricated through spray-coating the catalyst ink onto the carbon paper (1 cm × 1 cm). In detail, the catalyst ink was prepared by dispersing 10 mg of the prepared catalysts into a mixed solution containing 1 mL isopropyl alcohol and 45 μL Nafion solution with sonication for 1 h. Subsequently, the resulting catalyst ink was sprayed onto the carbon paper. Throughout the entire spraying process, the carbon paper was positioned on a heating plate set at 70℃ to rapidly evaporate the solvent and facilitate the formation of the working electrode.

Characterization

The crystal structures of the prepared samples were characterized by powder X-ray diffraction (XRD) spectroscopy with Cu Kα radiation (λ = 1.5418 Å, 40 kV and 40 mA) in the 2θ range of 10-90° at a scanning rate of 8°/min. The surface morphology and microstructure were observed by using field emission scanning electron microscope (FE-SEM, JSM-7001F, JEOL, Japan) and high-resolution transmission electron microscopy (HRTEM, JEM-2100F, JEOL, Japan). The surface element valence state and element composition were investigated by using X-ray photoelectron spectroscopy (XPS, Escalab 250Xi, Thermo Fisher Scientific, USA). The structure and chemical bonding were detected by Fourier Transform Infrared (FT-IR, Nicolet 5700). The recombination rate of the electron-hole pairs was determined by using photoluminescence spectroscopy (PL, F4500, Hitachi Corporation, Japan). CO_2-temperature-programmed desorption (CO_2-TPD) measurements were performed with the Belcat-II apparatus, equipped with a thermal conductivity detector (TCD).

Electrochemical measurements

The electrochemical CO_2RR measurements were performed in a three-channel flow cell connected to an electrochemical workstation at room temperature. The carbon paper uniformly deposited with catalysts was used as the working electrode. The Ag/AgCl electrode and Pt sheet were used as reference electrode and counter electrode, respectively. To ensure the proton exchange and avoid electrolyte outflow, the two compartments were separated by a Nafion 117 ion exchange membrane. This membrane ensured that only protons could pass through while blocking the migration of other ions. Once all the components of the flow cell were assembled,

1.0 M KOH electrolyte was circulated to fill both cathode and anode compartments at a flow rate of 12.5 sccm (mL/min) by using a peristaltic pump. Throughout the whole test, the high purity CO_2 gas was continuously fed into the electrolyte via a gas flow channel located behind the cathode compartment with a flow rate of 35 sccm. All mentioned potentials were converted to the reversible hydrogen electrode (RHE) by using the following Nernst equation:

$$E(\text{vs. RHE}) = E(\text{vs. Ag/AgCl}) + 0.197\ \text{V} + 0.059 \times \text{pH}$$

Analysis of CO_2 reduction products

The gaseous product products generated in the cathode compartment were analyzed by using an online gas chromatograph (Agilent 7890A GC System) equipped with a thermal conductivity detector (TCD) and a flame ionization detector (FID). During the test, Ar was used as the carrier gas. TCD was employed for the quantitative detection of H_2, while FID was used to detect CO, CH_4 and C_2H_4. The FEs of gas phase products at each applied potential were calculated according to the following equation:

$$FE_g = \frac{2 \times 96485(c/mol) \times V(mL/\text{min}) \times 10^{-6}(m^3/mL) \times v(vol\%) \times 1.013 \times 10^5(N/m^2)}{8.314(N{\cdot}m/mol{\cdot}K) \times 298.15(K) \times I_{total}(C/s) \times 60(s/\text{min})}$$

where v (vol %) is the volume concentration of CO detected by GC, V (mL/min) is the gas flow rate and I_{total} (C/s) is the measured steady state current density.

The liquid phase products were analyzed by ^{1}H nuclear magnetic resonance (NMR) spectroscopy (Bruker Avanceav III HD 500 MHZ). 500 μL of cathode electrolyte was mixed with 100 μL of deuterated water (D_2O) and 100 μL of DMSO solution used as an internal standard. The water suppression mode was implemented to minimize the influence of solvents. The FEs of liquid phase products were calculated as follows:

$$FE_L = \frac{ZFVC}{Q}$$

where Z is the electron transfer number, F is Faraday constant (96,485 C/mol), V is the volume of catholyte, C is the concentration of the liquid product and Q is the total charge consumed in the electrocatalysis.

In-situ Fourier transformed infrared spectroscopy (FT-IR).

The in situ ATR-SEIRAS measurements were performed on a Bruker Vertex 70 Fourier-transform infrared spectrometer equipped with a liquid-nitrogen-cooled mercury cadmium telluride (MCT/B) detector and a VeeMAX III ATR accessory (Pike Technologies). A custom three-electrode flow cell was employed, using a Pt plate and an Ag/AgCl electrode as the counter and reference electrodes, respectively. The catalyst ink was drop-cast onto a gold film deposited on a semi-cylindrical silicon prism, which functioned as the working electrode. The measurements were carried out in 1.0 M KOH electrolyte with continuous CO_2 purging at a flow rate of 35 sccm. Chronoamperometric measurements were performed by stepping the

potential from -0.2 V to −1.8 V in increments of -0.2 V, while corresponding ATR-SEIRAS spectra were collected at each potential. For reference, spectra were also recorded under open-circuit potential (OCP) conditions.

Density functional theory (DFT) calculations

The DFT calculations were performed using the Vienna Ab-initio Simulation Package (VASP).[3,4] The effective core potential is described by the projector augmented wave method, and the exchange correlation energy is calculated by using the Perdew-Burke-Ernzerhof (PBE) functional.[5] The geometry convergence tolerance for energy change and max force were 10^{-5} eV and 0.03 eV Å. $CdCO_3$ (110) and AgCl (100) surfaces contain four layers, and the bottom two layers is fixed while the top two layers are relaxed to reach the lowest total energy.[6,7] A vacuum layer of ~15 Å thick was added in the slab cell along the direction perpendicular to the surface to minimize the artificial interactions between the surface and its periodic images. The Gibbs free energy (G) of a species is calculated as G = E + ZPE -TS. Here, E is the total energy of a species obtained from DFT calculations, ZPE and S are the zero-point energy and entropy of a species respectively, and T= 298.15 K.

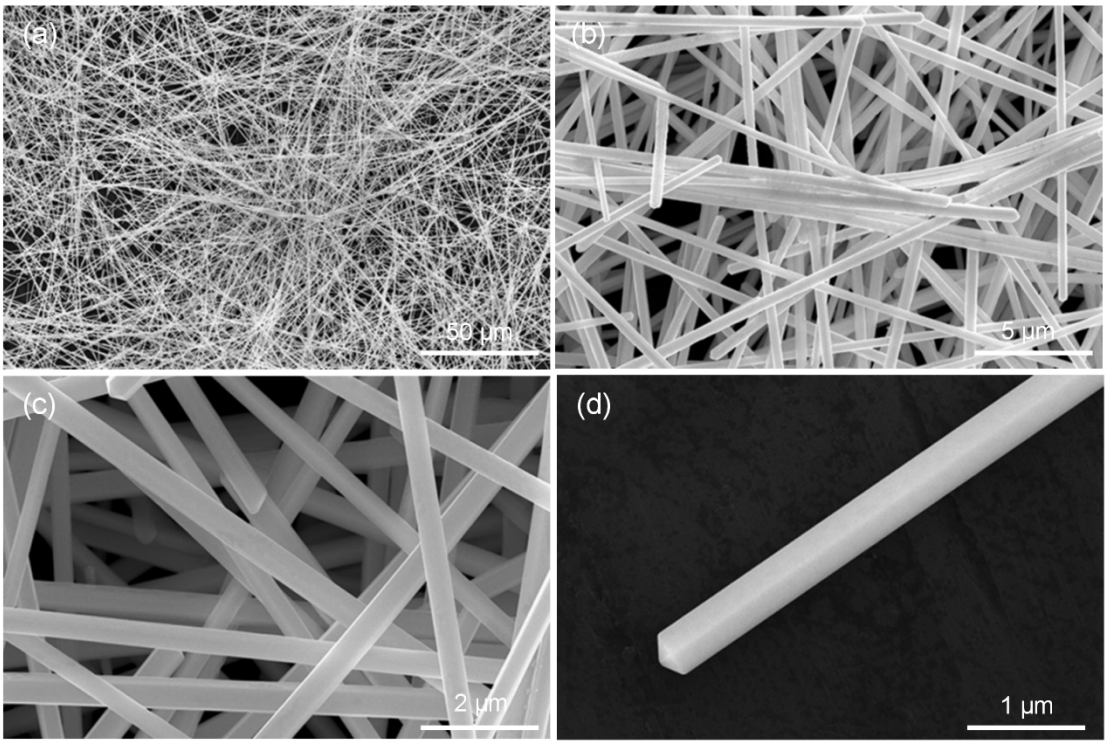

Fig. S1. SEM images of Ag NWs (a-d).

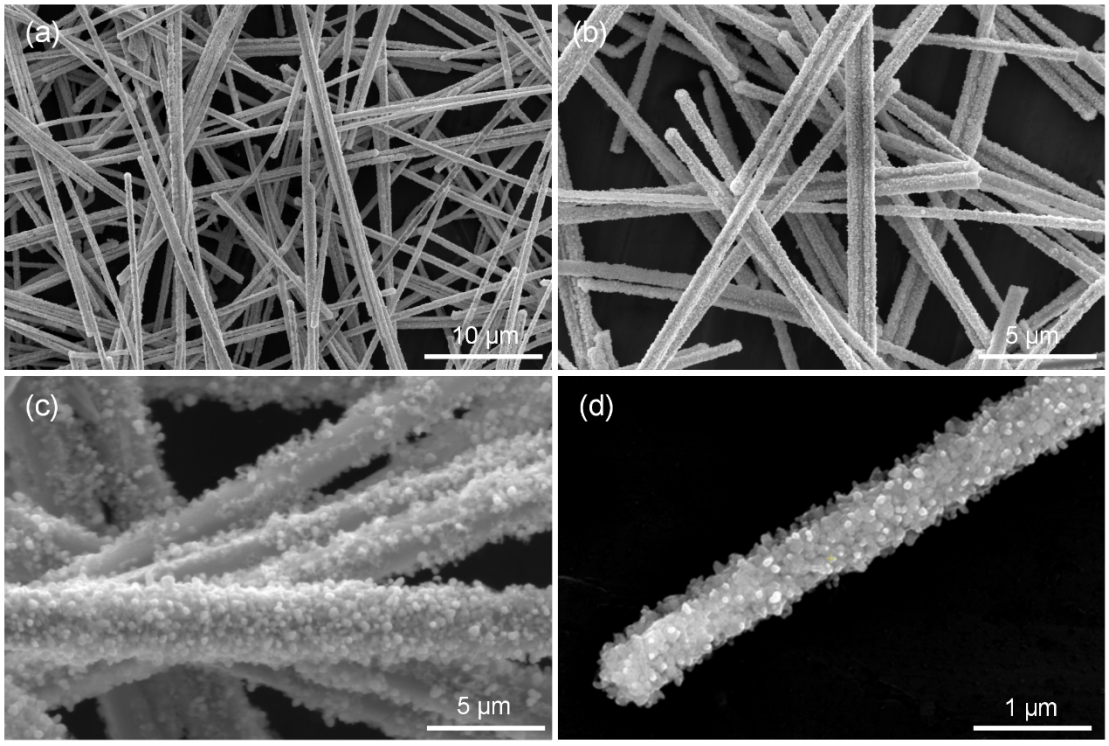

Fig. S2. SEM images of AgCl NWs (a-d).

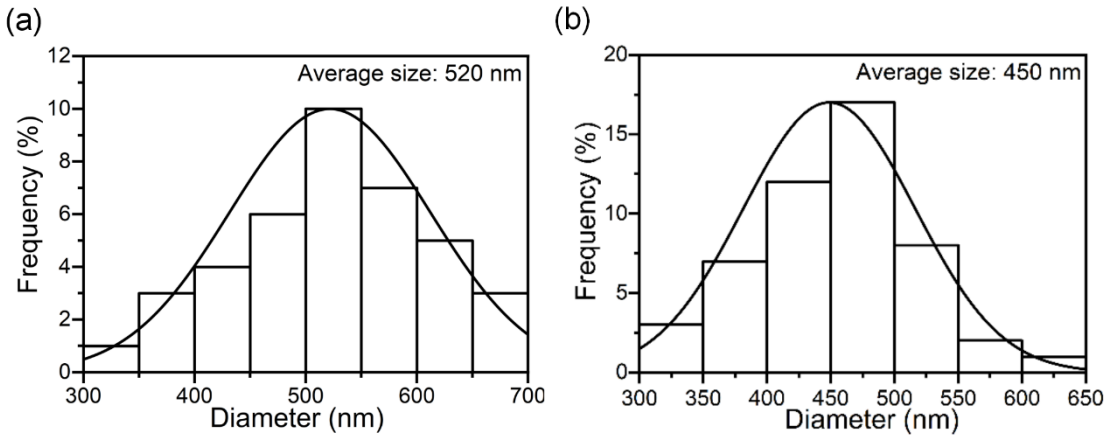

Fig. S3. Size distributions of Ag NWs (a) and AgCl NWs (b).

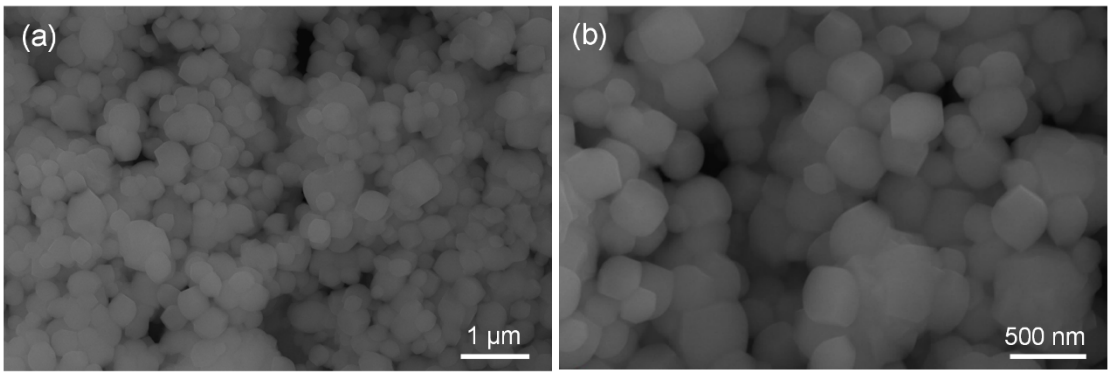

Fig. S4. SEM images of $CdCO_3$ (a and b).

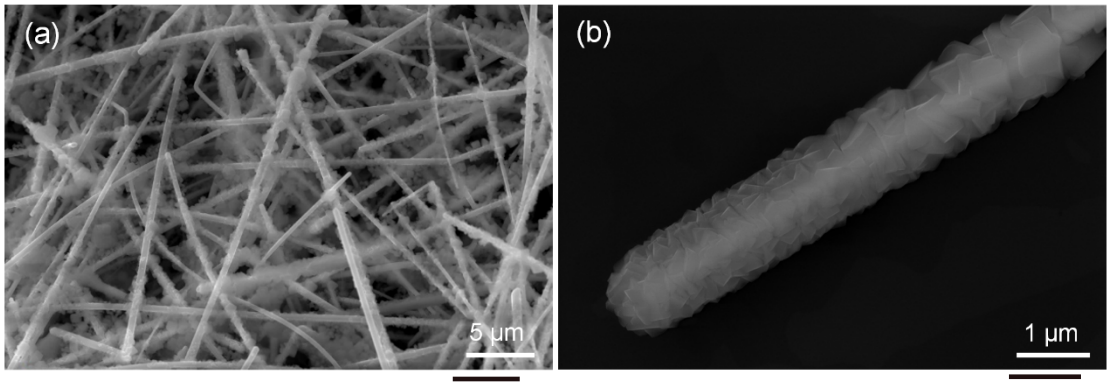

Fig. S5. SEM images of $CdCO_3$/Ag NWs (a and b).

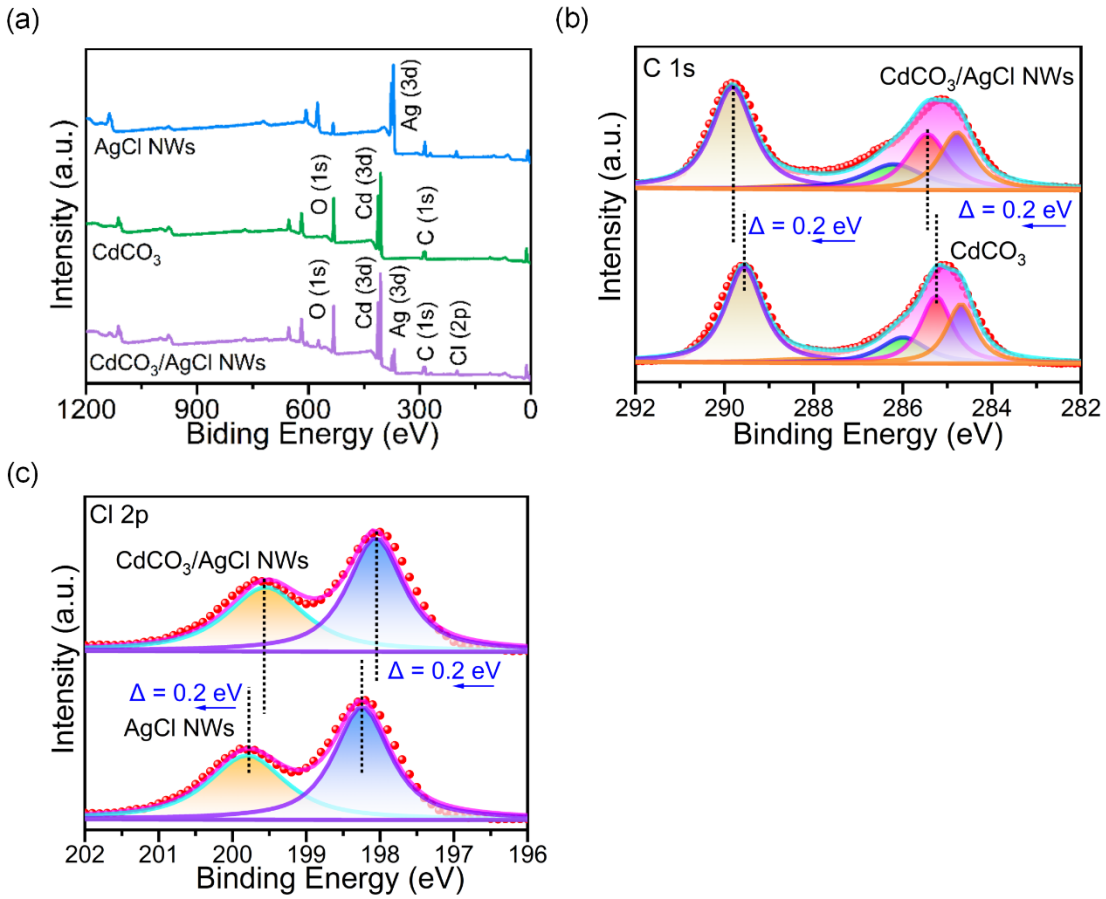

Figure S6. (a) XPS survey spectra of AgCl NWs, $CdCO_3$ and $CdCO_3$/AgCl NWs. (b) C 1s high resolution XPS spectra of $CdCO_3$ and $CdCO_3$/AgCl NWs. (c) Cl 2p high resolution XPS spectra of AgCl NWs and $CdCO_3$/AgCl NWs.

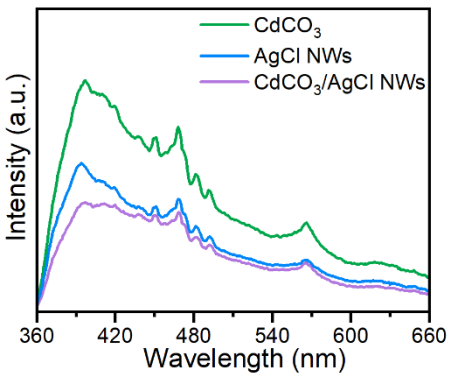

Figure S7. PL spectra of AgCl NWs, $CdCO_3$ and $CdCO_3$/AgCl NWs.

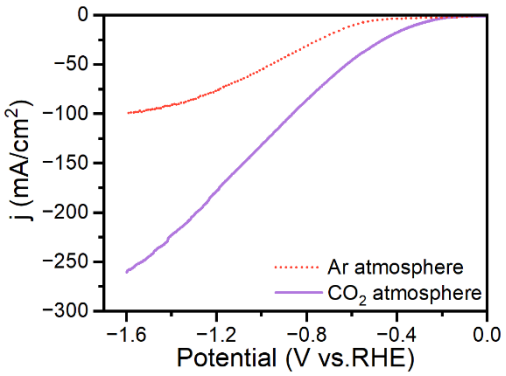

Figure S8. LSV curves of $CdCO_3$/AgCl NWs under Ar- and CO_2- atmosphere.

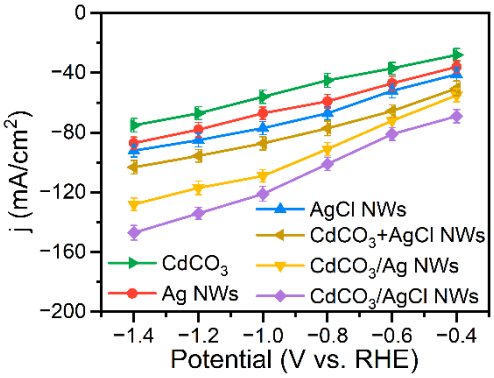

Figure S9. Partial current densities of the prepared samples at different applied potentials.

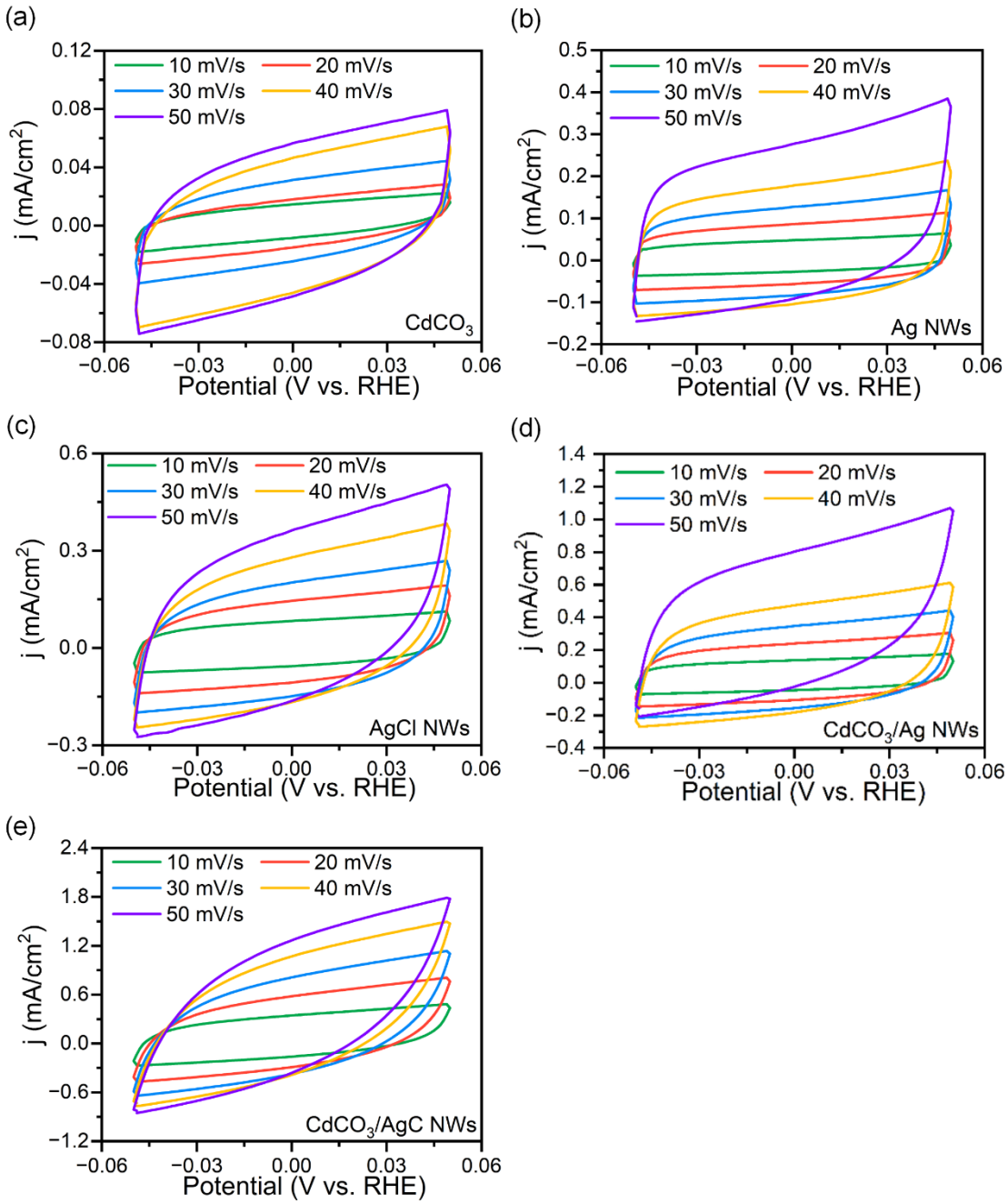

Figure S10. Cyclic voltammertrys (CV) curves at different scan rate (10-50 mV/s) for $CdCO_3$ (a), Ag NWs (b), AgCl NWs (c), $CdCO_3$/Ag NWs (d) and $CdCO_3$/AgCl NWs (e).

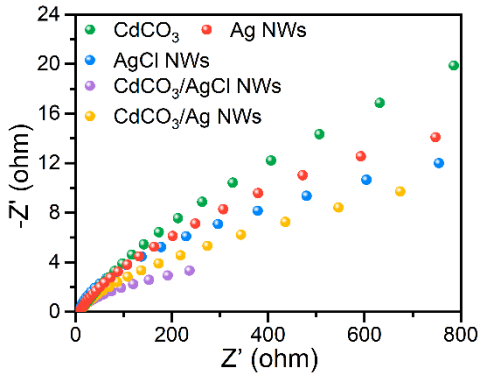

Figure S11. EIS curves for $CdCO_3$, Ag NWs, AgCl NWs, $CdCO_3$/Ag NWs and $CdCO_3$/AgCl NWs.

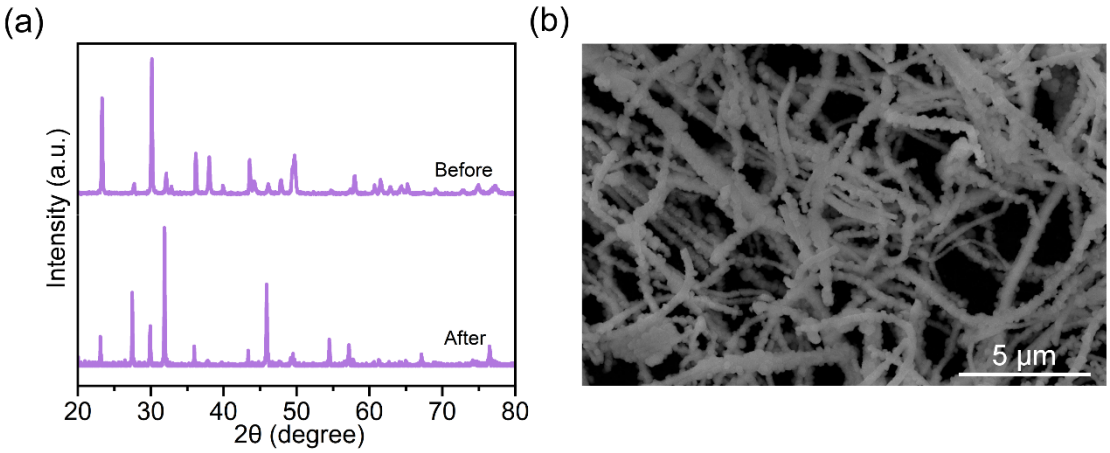

Figure S12. (a) XRD patterns of $CdCO_3$/AgCl NWs before and after electrolysis. (b) SEM image of $CdCO_3$/AgCl NWs after electrolysis.

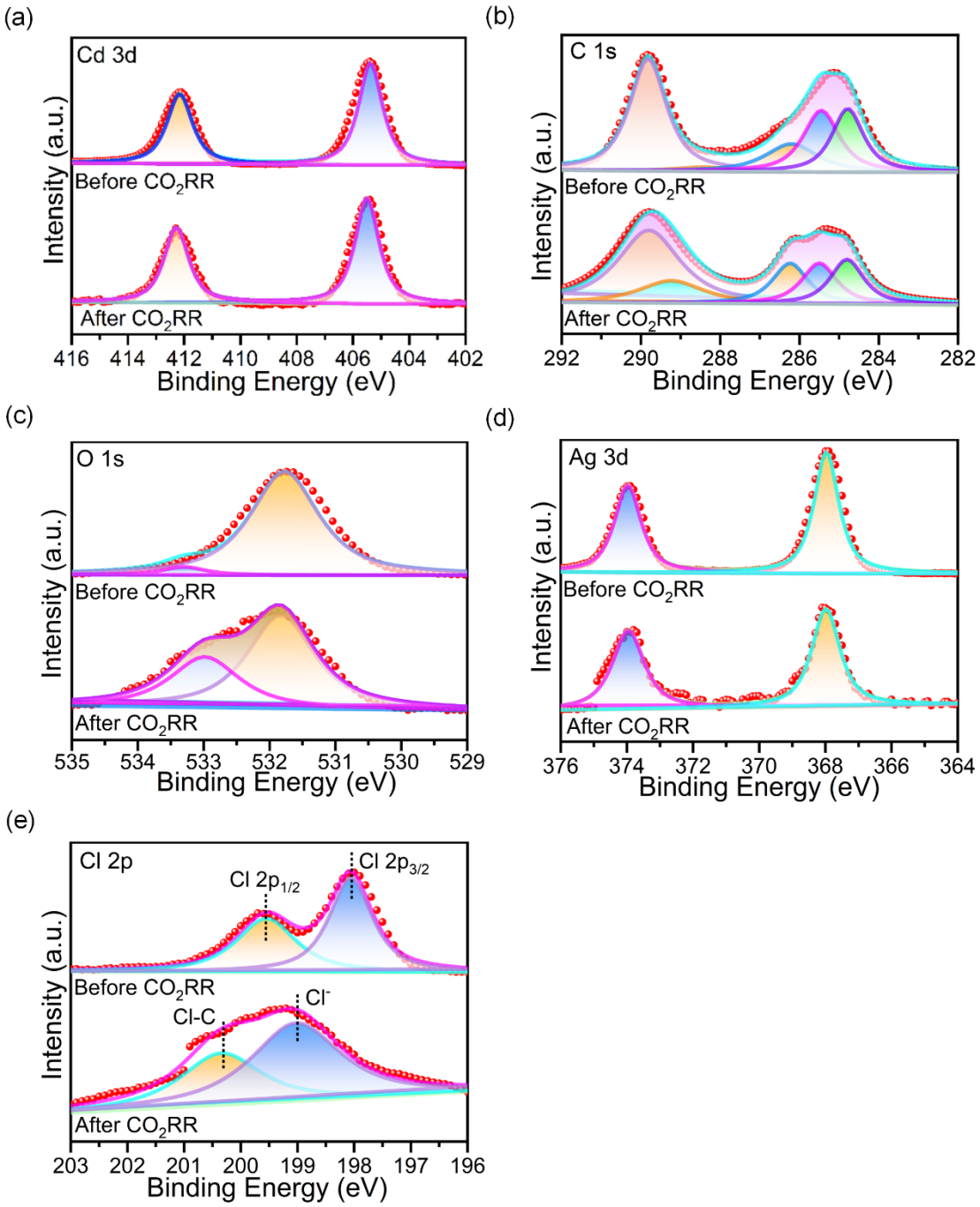

Figure S13. High resolution XPS spectra of (a) Cd 3d, (b) C 1s, (c) O 1s, (d) Ag 3d and Cl 2p (2) for $CdCO_3$/AgCl NWs before and after electrocatalytic CO_2RR stability test.

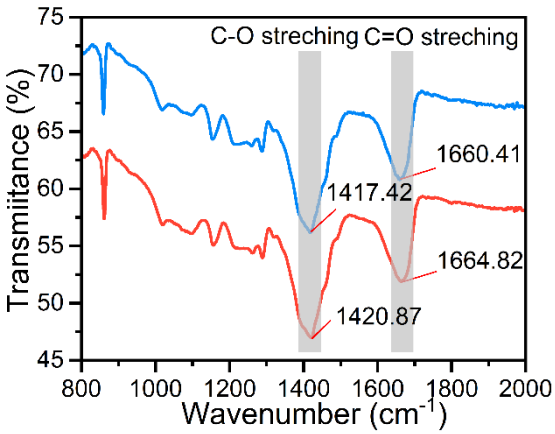

Figure S14. Fourier transform infrared spectroscopy (FTIR) of $CdCO_3$/AgCl NWs before and after electrocatalytic CO_2RR stability test.

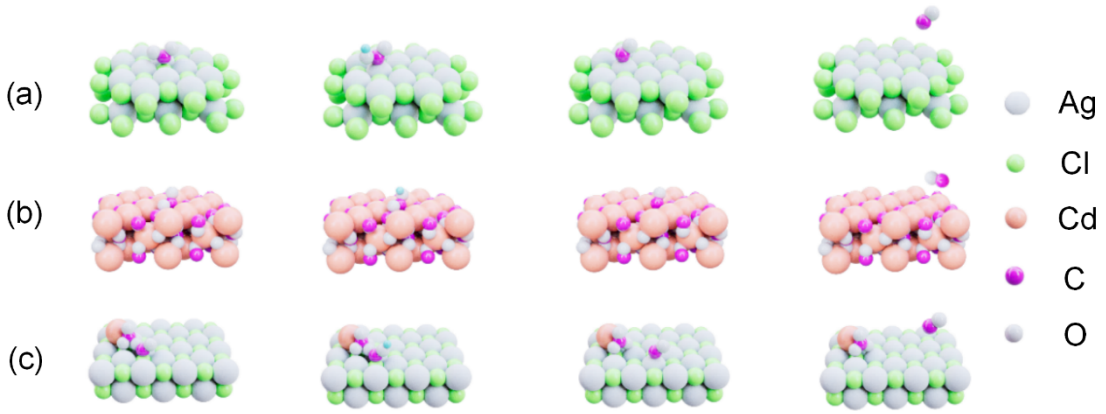

Figure S15. The optimized intermediates adsorption structures over (a) AgCl NWs, (b) $CdCO_3$ and (c) $CdCO_3$/AgCl NWs surfaces.

Table. S1. The performance comparison of this work with the state-of-the-art results.

Catalysts	FE_{CO} (%)	Potential (V vs. RHE)	Reference
$CdCO_3$/AgCl NWs	97.14	-1.0	This work
nanoZnF_2	82	-1.05	[8]
Fe-$N_{5\text{-pyrro}}$	96.6	-1.4	[9]
$Zn_{1.5}Mg_{1.5}Al_1$-LDH	91.8	-1.4	[10]
N^1P^3CA	91.44	-1.2	[11]
Ni, Fe-N-C	92.37	-1.0	[12]
ZIF-8/Zn-40	91.8	-1.9	[13]
TA-ZnS	83	-1.9	[14]
Cd/$Cd(OH)_2$/CP	98.3	-2	[15]
Cu_8Pd_2	88	-0.97	[16]
$IL_{10\%}$@ZIF-8	96	-1.2	[17]
$Ag_{1.0}$-ApmimBr$_{1.5}$/KB	95.1	-0.9	[18]
PIL-Cl@AgOAC-1.0	96.8	-0.91	[19]

References

(1) M. Parente, M.V. Helvert, R.F. Hamans, R. Verbroekken, R. Sinha, A. Bieberle-Hütter, A. Baldi, *Nano Lett.*, 2020, **20**, 5759-5764.

(2) S.-J. Kim, S.-C. Lee, C. Lee, M.H. Kim, Y. Lee, *Nano Energy*, 2018, **48**, 134-143.

(3) G. Kresse, J. Hafner, *Phys. Rev. B*, 1993, **48**, 13115-13118.

(4) G. Kresse, J. Furthmüller, *Phys. Rev. B*, 1996, **54**, 169-186.

(5) J.P. Perdew, K. Burke, M. *Phys. Rev. Lett.*, 1996, **77**, 3865-3868.

(6) S. Grimme; J. Antony; S. Ehrlich; H. Krieg, *J. Chem. Phys.*, 2010, **132**, 154104.

(7) H.J. Monkhorst, J.D. Pack, *Phys. Rev. B*, 1976, **13**, 5188-5192.

(8) H.-C. Wu, C.-C. Lin, C.-Hs. Yang, Y.-W. Huang, C.-H. Yeh, Y.-J. Chou, T.-C. Liu, *Chem. Eng. J.*, 2025, **509**, 161002.

(9) D. Li, J.B. Liu, X.Y. Chen, Z.M. Feng, S.H. Wang, Y.C. Wang, N. Lin, J. Wu, Y.J. Feng, *Appl. Catal. B Environ. Energy*, 2025, **365**, 124824.

(10) X.J. Ma, T.X. Liu, B.M. Lu, Y.P. Zhang, *J. Alloys Compd.*, 2024, **973**, 172858.

(11) Y.F. Yan, H.Z. Wang, X.Z. Bi, Y.Z. Zhao, M.B. Wu, *Chem. Commun.*, 2024, **60**, 6439–6442.

(12) Y. Sun, K.Y. Chen, K. Zhao, B.D. Chai, X.L. Wang, W. Wang, *J. Environ. Chem. Eng.*, 2022, 10, 108986.

(13) R.J. Zhang, J. Yang, X.B. Zhao, H. Yang, H.P. Li, B.R. Ji, G.Y. Zhou, X.X. Ma, D.X. Yang, *ChemCatChem*, 2022, **14**, e202101653.

(14) H.-i. Nam, K.R. Park, Y.-W. Choi, H.-j. Sim, K.Y. Sohn, D.-H. Lim, *Appl. Surf. Sci.*, 2023, **612**, 155646.

(15) X.Y. Jia, K.S. Qi, J. Yang, Z.X. Fan, Z.X. Hua, X.Q. Wan, Y.H. Zhao, Y.D. Mao, D.X. Yang, *Chem. Eur.* J., 2023, **29**, e202302613.

(16) D. Chen, Y.L. Wang, D.Y. Liu, H. Liu, C. Qian, H.Y. He, J. Yang, *Carbon Energy*, 2020, 2, 443–451.

(17) Y.W. Chen, T. Zheng, H. Liu, W.D. Xie, J.L. Huang, Y.M. Wang, X.Y. Zhang, Z. Yuan, Z.L. Xiong, *Appl. Surf. Sci.*, 2026, **719**, 165076.

(18) Y. Shi, H. Tang, Z.Z. Wei, T. Wang, P. Li, Z.H. Liu, X.Y. Zhang, C. Liang, *Mater. Sci. Eng. B*, 2025, **321**, 118505.

(19) G.-Y. Duan, X.-Q. Li, Y.-R. Du, B.-H. Xu, *Chem. Eng. J.*, 2023, **455**, 140910.